Water-Based Coherent Detection of Broadband Terahertz Pulses

Yong Tan,[1,2,6,§] Hang Zhao,[2,§] Wei-Min Wang,[3,*] Rui Zhang,[4] Yue-Jin Zhao,[2,†] Cun-Lin Zhang,[1] Xi-Cheng Zhang,[5] and Liang-Liang Zhang[1,‡]

[1]*Key Laboratory of Terahertz Optoelectronics (MoE), Department of Physics, Capital Normal University, Beijing 100048, China*

[2]*Beijing Key Laboratory for Precision Optoelectronic Measurement Instrument and Technology, School of Optics and Photonics, Beijing Institute of Technology, Beijing 100081, China*

[3]*Department of Physics and Beijing Key Laboratory of Opto-electronic Functional Materials and Micro-nano Devices, Renmin University of China, Beijing 100872, China*

[4]*Shenzhen Institute of Advanced Technology, Chinese Academy of Sciences, Shenzhen 518055, China*

[5]*The Institute of Optics, University of Rochester, Rochester, New York 14627, USA*

[6]*Research Center for Metamaterials, Wuzhen Laboratory, Jiaxing 314500, China*

(Received 25 August 2021; revised 15 November 2021; accepted 11 February 2022; published 4 March 2022)

Both solids and gases have been demonstrated as the materials for terahertz (THz) coherent detection. The gas-based coherent detection methods require a high-energy probe laser beam and the detection bandwidth is limited in the solid-based methods. Whether liquids can be used for THz detection and relax these problems has not yet been reported, which becomes a timely and interesting topic due to the recent observation of efficient THz wave generation in liquids. Here, we propose a THz coherent detection scheme based on liquid water. When a THz pulse and a fundamental laser beam are mixed on a free-flowing water film, a second harmonic (SH) beam is generated as the plasma is formed. Combining this THz-induced SH beam with a control SH beam, we successfully achieve the time-resolved waveform of the THz field with the frequency range of 0.1–18 THz. The required probe laser energy is as low as a few microjoules. The sensitivity of our scheme is 1 order of magnitude higher than that of the air-based method under comparable detection conditions. The scheme is sensitive to the THz polarization and the phase difference between the fundamental and control SH beams, which brings direct routes for optimization and polarization sensitive detection. Energy scaling and polarization properties of the THz-induced beam indicate that its generation can be attributed to a four-wave mixing process. This generation mechanism makes simple relationships among the probe laser, THz-induced SH, and THz field, favorable for robustness and flexibility of the detection device.

DOI: 10.1103/PhysRevLett.128.093902

Terahertz (THz) time-domain spectroscopy (TDS) has been widely applied in biomedical research [1–3], material characterization [4–7], and ultrafast science [8–11]. Time-resolved coherent detection with simultaneous measurement of THz field amplitude and phase is the key feature of TDS. The most commonly used techniques for THz coherent detection include photoconductive antenna [12,13] and electro-optic sampling (EOS) [14,15] in solid media. The detection bandwidths of these two techniques are largely limited by the noninstantaneous response of carriers in semiconductor materials [4] and the phonon absorption in electro-optic crystals [16–18], respectively. By significantly decreasing the crystal thickness in EOS, the bandwidth can be broadened to 0.1–5 or 0.1–10 THz in ultrathin ZnTe or GaP crystal, respectively. However, this is at the expense of response sensitivity and additional complex correction to the response function near the crystal Restrahlen band [17,19,20]. In this case, it is difficult to obtain high signal-to-noise ratio (SNR) for high frequency components.

Because of the absence of the Restrahlen band and low dispersion, a gas medium irradiated by a near-infrared femtosecond (fs) laser has been demonstrated to coherently detect a broadband THz pulse (0.1–15 THz) with a smooth response function [21–25]. In 2006, Dai *et al.* mixed a THz-induced second harmonic (TISH) field with white light from the laser-excited air plasma and realized time-resolved THz coherent detection [21]. Then Liu *et al.* further reported the application of this air-based detection method in THz remote sensing in 2010 [23]. On this basis, the successive developments of air biased coherent detection (ABCD) [24] and optical field biased coherent detection (OBCD) [25] greatly improved the performances of the air-based detection scheme. The main mechanism is based on the third-order optical nonlinearity in excited air plasma, in which two fundamental fields (E_ω) and one THz field with a frequency much lower than ω mixed together to generate one second harmonic field ($E_{2\omega}$). To further improve the sensitivity, a gas medium with larger nonlinear

 © 2022 American Physical Society

susceptibility or higher gas pressure was also adopted [26–28]. In this gas-based detection scheme, the plasma formation is necessary [29], which usually requires the near-infrared probe laser energy with a few hundred microjoules (μJs) due to the high ionization threshold in the gas medium.

Liquid usually has a lower ionization threshold than gas [30–32] and a higher density close to solid, which means that light could interact with more molecules and it is easier to form high-density plasma. Moreover, most nonlinear phenomena during filamentation in liquid become much more remarkable than gas due to larger nonlinear susceptibility [33,34]. Therefore, it is natural to raise the question of whether liquid can provide THz coherent detection with lower probe laser energy and higher sensitivity. A few recent experiments have demonstrated strong broadband THz generation from water in a cuvette [35], a water film [36], and a water line [37], respectively. Although the THz generation mechanism in water demands clarification, it is clear that plasma excitation is necessary for THz generation, which is similar in air. Note that usually a THz generation process could be reversed for THz detection, so it is reasonable to expect that liquid, particularly water, could be harnessed as a high-performance THz detector with superior properties.

Here, we demonstrate a coherent detection scheme of broadband THz pulses in liquid water. We obtain the temporal waveform of a THz field with the frequency range of 0.1–18 THz by combining a TISH beam generated in water plasma with a control SH (CSH), where we prove that the generation mechanism of the TISH can be attributed to the four-wave mixing. Compared to the air-based detection, our proposed water-based scheme is well implemented with a much lower probe laser energy of even a few μJs and the detection sensitivity is 1 order of magnitude higher under the comparable conditions. This is the first time we realize a THz coherent detection scheme based on liquid and this scheme makes THz detection more achievable due to the low probe laser energy requirement. Hence, our scheme is favorable for situations in the absence of high enough probe laser energy, particularly when the probe laser beam needs to propagate a long distance to mix with the THz field and the beam energy is significantly depleted in the optical path.

Experimental setup.—Schematic of our experimental setup is depicted in Fig. 1(a). A THz pulse with the frequency range of 0.1–18 THz and an 800 nm fs probe beam with the same polarization along the vertical direction are co-focused on a 90-μm-thick free-flowing water film [36], and a water plasma is formed if the probe beam is above 2 μJ. Then, the 400 nm SH beam emitted from the water plasma is measured by a photomultiplier tube (PMT) through a 400 nm narrow-band filter. When a 50-μm-thick type-I β-barium borate (BBO) crystal is placed in the path of the 800 nm probe beam, a CSH beam can be generated and collinearly propagates with the fundamental beam. When the CSH beam is vertically polarized and coherent with the TISH beam, a linear component positively correlated with the THz field appears in the collected signal. This provides an opportunity to measure the THz field amplitude and phase simultaneously. To demonstrate the feasibility of this water-based detection scheme, we

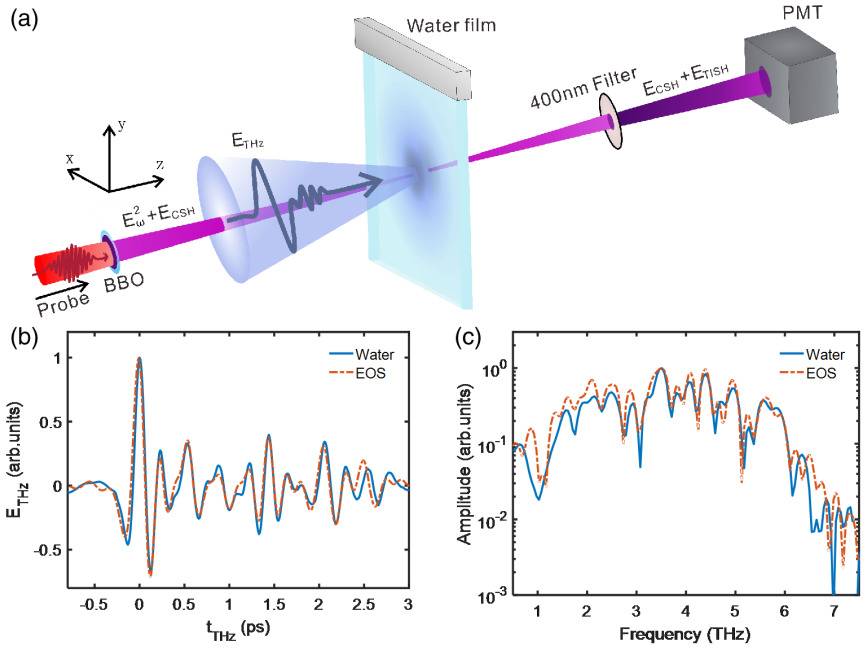

FIG. 1. Coherent detection of THz field by water film. (a) Schematic of the experimental setup. An 800 nm laser beam passes through a BBO crystal to generate a CSH of 400 nm and a THz pulse is focused on a water film to generate the other SH (i.e., TISH). Combining the TISH with CSH, the signal is collected by the PMT. (b),(c) Measured THz waveforms and the corresponding spectra, where the blue solid and red broken lines in each plot correspond to the results of water-based scheme and EOS with a GaP crystal, respectively.

measure a THz time-domain waveform and its corresponding spectrum, as shown by the blue solid lines in Figs. 1(b) and 1(c), respectively. The probe beam energy is set as 5 μJ in this experiment.

To compare the measured results with EOS, we limit the bandwidth of the THz pulse below 6 THz by using a low-pass filter and control the THz field strength at 0.3 MV/cm to ensure the detection validity based on the 100-μm-thick GaP crystal. By taking the complex response function into account, we reconstruct the waveform and spectrum of the THz pulse [15,17,19,20], as shown by the red broken lines in Figs. 1(b) and 1(c). The measured results of the THz waveforms and spectra from two detection methods agree well, which proves the reliability of the water-based coherent detection. Note that the structured spectrum in Fig. 1(c) results from the absorption of water vapor rather than liquid water [38], thus, the characteristic absorption lines of the two methods are almost the same. The introduction of the liquid water film would not obviously change the water vapor concentration and meanwhile, the humidity is kept constant in our laboratory.

TISH generation mechanism.—A four-wave mixing process is the basis of the air-based THz coherent detection, which is trigged to generate TISH carrying the THz field information. Analogously, one can expect that four-wave mixing can also arise in water since it has a higher third-order nonlinear coefficient than air. The four-wave mixing gives the dependency of the TISH field E_{TISH} on the probe laser field E_{ω} and the THz field E_{THz} as: $E_{\mathrm{TISH}} = \chi^{(3)} E_{\omega}^{2} E_{\mathrm{THz}}$, where $\chi^{(3)}$ is the third-order nonlinear coefficient. The TISH energy signal sampled at a time point t_{THz} can be given by

$$\varepsilon_{\mathrm{TISH}}(t_{\mathrm{THz}}) \propto \int |\chi^{(3)} E_{\mathrm{THz}}(t) E_{\omega}^{2}(t - t_{\mathrm{THz}})|^{2} dt. \quad (1)$$

The TISH energy is proportional to the THz intensity $E_{\mathrm{THz}}^{2}(t_{\mathrm{THz}})$, and therefore induces an incoherent detection. The TISH energy signal calculated from Eq. (1) is shown by the red broken line in Fig. 2(a), which reflects the THz intensity profile. The blue line illustrates the measured signal without the BBO crystal placed in the probe beam (i.e., without the CSH), which approaches the calculated results shown by the red broken line. In this experiment, the THz pulses with the strength of 1 MV/cm and the frequency range of 0.1–18 THz are used. The inset of Fig. 2(a) displays that the dependency of the TISH energy on the THz field strength is quadratic and in agreement with Eq. (1). These results together with the THz polarization dependence shown below indicate that the underlying mechanism can be attributed to the four-wave mixing.

Coherent detection of THz pulses.—In order to realize coherent detection, we introduce a CSH beam by placing a BBO crystal in the optical path of the probe beam. The CSH beam is spatiotemporally overlapped with the TISH beam.

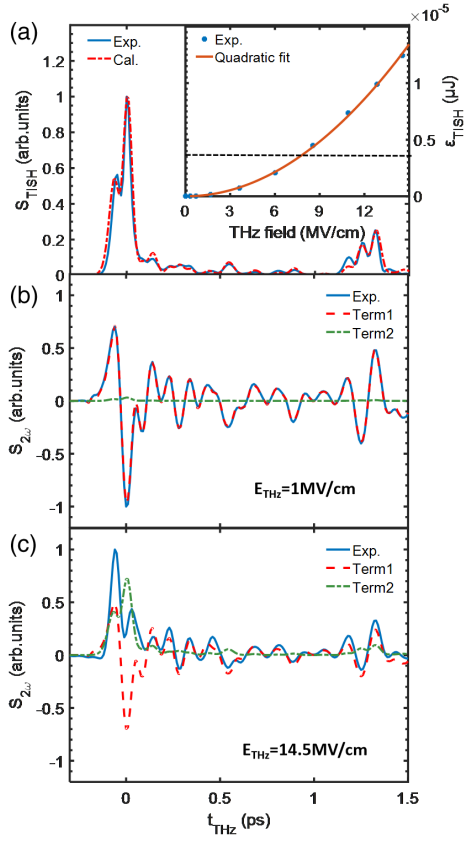

FIG. 2. TISH energy signal and interference signals from the water film. (a) Measured (blue solid line) and calculated (red broken line) TISH energy signals without the CSH imposed in the detection. Inset shows the TISH energy as a function of the THz field strength, where a quadratic fit is presented by the red solid line. The black broken line in the inset marks the CSH energy used in the experiments of Figs. 2(b) and 2(c). (b), (c) Interference signals of the TISH and CSH, where the THz field strength is taken as 1 MV/cm and 14.5 MV/cm, respectively. The blue solid line shows the measured result, and the red and green broken lines correspond to the calculation results of the first term (coherent component) and second term (incoherent component) in Eq. (2), respectively.

When the polarization directions of the CSH and TISH beams are parallel, the measured signal at a time point t_{THz} can be expressed as the interference of the two beams:

$$\begin{aligned} S_{2\omega}(t_{\mathrm{THz}}) &\propto \int_{-\infty}^{+\infty} |E_{\mathrm{TISH}} + E_{\mathrm{CSH}}|^{2} dt \\ &\propto 2\,\mathrm{Re}\left\{ \int_{-\infty}^{+\infty} \chi^{(3)} E_{\omega}^{2}(t - t_{\mathrm{THz}}) E_{\mathrm{CSH}}^{*}(t - t_{\mathrm{THz}}) E_{\mathrm{THz}}(t) dt \right\} \\ &\quad + \int_{-\infty}^{+\infty} |\chi^{(3)} E_{\omega}^{2}(t - t_{\mathrm{THz}}) E_{\mathrm{THz}}(t)|^{2} dt \\ &\quad + \int_{-\infty}^{+\infty} E_{\mathrm{CSH}}(t - t_{\mathrm{THz}}) E_{\mathrm{CSH}}^{*}(t - t_{\mathrm{THz}}) dt \end{aligned} \quad (2)$$

The first term is linearly proportional to the THz field and gives a phase-resolved cross-correlation measurement, which introduces the coherent detection. The second term leads to the incoherent detection and has been discussed in Eq. (1). The third term is a constant background and can be experimentally excluded by lock-in detection. To clarify the contributions of the first two terms, we purposely set the energy of the CSH beam as 3.5×10^{-6} μJ, which is equal to the TISH energy induced by the THz field of 7.5 MV/cm. It is marked by the black broken line in the inset of Fig. 2(a). When the THz field strength is 1 MV/cm and the CSH energy is nearly 2 orders of magnitude stronger than the TISH energy, the coherent component predicted by the first term in Eq. (2) is dominant. As shown in Fig. 2(b), the measured signal agrees very well with the result calculated by the first term. If we consider the detection with coherent component 10 times higher than the incoherent component as sufficiently coherent, the energy ratio between the CSH and TISH should be larger than 25 (The validation of this criterion can be seen in Supplemental Figs. S1 and S2 [39]). While the TISH energy is higher, e.g., Fig. 2(c) with the THz field strength of 14.5 MV/cm, the incoherent component (green broken line) is at the similar level to the coherent component (red broken line), and hence the measured signal (blue solid line) deviates from the results of the coherent detection.

Note that the maximum SH conversion efficiency of the BBO crystal is ~5% and the CSH energy can reach around 0.25 μJ with the probe beam of 5 μJ. This CSH energy is 5 orders of magnitude stronger than 3.5×10^{-6} μJ used in the experiments of Figs. 2(b) and 2(c). Therefore, it is quite easy to achieve coherent detection of strong THz pulses, which demands the energy ratio between the CSH and TISH larger than 25. For example, the required CSH energy is only 3.3×10^{-4} μJ to coherently detect the THz field of 14.5 MV/cm, which is the highest field strength available in our experiments (Please see more results of coherent detection shown in Supplemental Figs. S1 and S2 [39]). Even when the THz field strength is as high as 100 MV/cm, the required CSH energy of 1.55×10^{-2} μJ is very easy to achieve.

Phase and polarization dependencies.—We focus on the coherent detection with the energy ratio between the CSH and TISH larger than 25. In this case, the measured time-resolved signal at a time point t_{THz} reduces to

$$S_{2\omega}^{\mathrm{coherent}}(t_{\mathrm{THz}}) \propto \mathrm{Re}\left\{\int_{-\infty}^{+\infty} \chi^{(3)} E_{\omega}^{2}(t-t_{\mathrm{THz}}) E_{\mathrm{CSH}}^{*}(t-t_{\mathrm{THz}}) E_{\mathrm{THz}}(t) dt\right\}.$$

We define $E_{\omega}^{2}(t)E_{\mathrm{CSH}}^{*}(t) = I_{\omega}(t)\sqrt{I_{\mathrm{CSH}}(t)}\exp(i\Delta\varphi)$, where the relative phase $\Delta\varphi = 2\varphi_{\omega} - \varphi_{\mathrm{CSH}}$ with φ_{ω} and φ_{CSH} denoting the phases of the probe and CSH beams, respectively. The signal at a time point t_{THz} can be expressed by

$$\begin{aligned} S_{2\omega}^{\mathrm{coherent}}(t_{\mathrm{THz}}) \propto \cos(\Delta\varphi) & \int_{-\infty}^{+\infty} I_{\omega}(t-t_{\mathrm{THz}})\sqrt{I_{\mathrm{CSH}}(t-t_{\mathrm{THz}})}\,\mathrm{Re}[E_{\mathrm{THz}}(t)]dt \\ & + \sin(\Delta\varphi)\int_{-\infty}^{+\infty} I_{\omega}(t-t_{\mathrm{THz}})\sqrt{I_{\mathrm{CSH}}(t-t_{\mathrm{THz}})}\,\mathrm{Im}[E_{\mathrm{THz}}(t)]dt. \end{aligned}$$

For a given frequency component of the THz field, $\mathrm{Im}[E_{\mathrm{THz}}(t)] = \mathrm{Re}\{E_{\mathrm{THz}}[\omega_{\mathrm{THz}}t + (\pi/2)]\}$ and the signal at a time point t_{THz} can then be written by

$$\begin{aligned} S_{2\omega}^{\mathrm{coherent}}(t_{\mathrm{THz}}) \propto & \cos(\Delta\varphi)\,\mathrm{Re}[E_{\mathrm{THz}}(t_{\mathrm{THz}})] \\ & + \sin(\Delta\varphi)\mathrm{Re}\left[E_{\mathrm{THz}}(t_{\mathrm{THz}})\exp\left(\frac{i\pi}{2}\right)\right]. \quad (3) \end{aligned}$$

Obviously, the measured signal can accurately reproduce the time-resolved THz field when $\Delta\varphi = 0$. Besides, Eq. (3) allows us to further investigate the properties of our detection scheme by adjusting $\Delta\varphi$. To capture the full dependence of the measured signal on the relative phase, we record the THz time-domain waveforms while translating the BBO crystal along the optical path to control $\Delta\varphi$ (see Supplemental Material, Fig. S5 [39]). The experimental results are consistent with the calculations predicted by Eq. (3).

To further demonstrate that the scheme is sensitive to the THz polarization, we study the dependency of the TISH energy and interference signals on the relative polarization angle θ between the probe beam and THz field. In the experiment, the probe beam is vertically polarized (y direction) and the THz polarization is rotated, where the THz propagation is along the z direction. Water is an isotropic medium, and two elements $\chi_{yyyy}^{(3)}$, $\chi_{xxyy}^{(3)}$ of its third order susceptibility $\chi^{(3)}$ can describe the polarization-sensitive signals, where the four subscripts represent the polarizations of 2ω (TISH), THz, ω, and ω waves, respectively. The TISH energy versus θ without the CSH beam imposed in the probe beam is shown in Fig. 3(a). The vertical component of TISH energy corresponding to $\chi_{yyyy}^{(3)}$ follows $\cos^2\theta$. The horizontal component of TISH energy corresponding to $\chi_{xxyy}^{(3)} \approx \frac{1}{3}\chi_{yyyy}^{(3)}$ is also observed, which follows $\sin^2\theta$ (see details in Supplemental Material [39]).

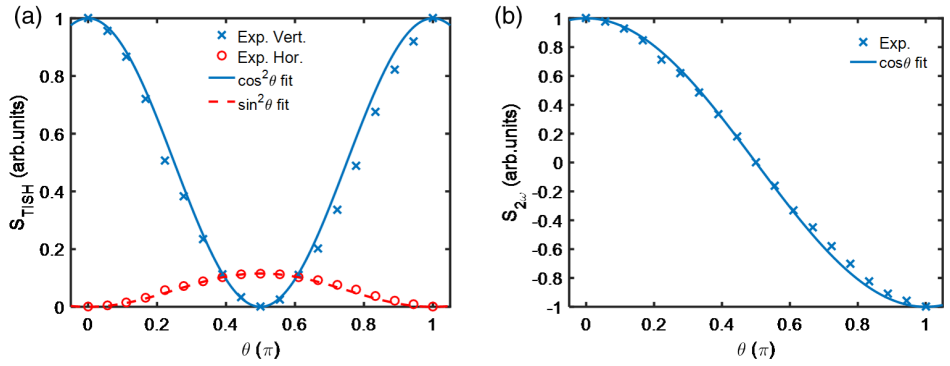

FIG. 3. Dependence of the measured signal on THz polarization. (a) TISH energy as a function of the relative polarization angle θ between the probe laser and THz fields, where the crosses and dots correspond to the vertical and horizontal components, respectively. (b) Measured signal as a function of θ in the case of the coherent detection.

Figure 3(b) shows the dependency of the interference signal on θ when the CSH beam is applied to ensure the coherent detection and its polarization is vertical. It follows $\cos\theta$ and agrees with the first term in Eq. (2). The results indicate that our scheme can provide polarization sensitive detection and two orthogonal components of the THz field could be time-resolved detected by properly rotating the polarization of the probe beam.

Comparison with the air-based detection.—Our water-based scheme requires much lower probe laser energy than the air-based detection scheme [21–25] to generate the same level of TISH. We employ ~5 μJ probe beam to measure the waveform of a 1 MV/cm THz field in the range of 0.1–18 THz in the water film, as shown in the blue line in Fig. 4(a). In the air-based scheme, the energy of the probe beam should be enhanced to ~75 μJ to coherently detect the THz field [the red broken line in Fig. 4(a)] at the same leveled SNR. A clearer comparison of the two schemes can be seen in Fig. 4(b), which shows that 1 to 2 orders of magnitude higher probe beam energy is needed in air to achieve the same level of TISH energy. In other words, the detection sensitivity in water is 1 to 2 orders of magnitude higher than that in air under the comparable experimental conditions. For example, if a 35 μJ probe laser beam is applied, a 0.3 MV/cm THz field can induce 3.1×10^{-8} μJ TISH beam in water, but the value of TISH is only 0.05×10^{-8} μJ in air. With these TISH beams adopted in the coherent detection, the signal to noise ratios (SNRs) are ~85:1 and ~10:1 for the water-based and air-based schemes, respectively. More data can be seen in Figs. S3, S6 in the Supplemental Material [39]. Note that even when the energy is reduced to 2 μJ, the THz signal is still able to be observed with a lowered SNR (see Supplemental Fig. S4 [39]).

In summary, our investigation has shown for the first time that liquid can be used for coherent detection of THz pulses. The water-based scheme with a reduced probe laser energy and enhanced sensitivity provides a reliable coherent detection of broadband THz fields, relaxing the existing problems in the solid- and air-based schemes. We have achieved the time-domain waveform of the THz field with the frequency range of 0.1–18 THz, and, in principle, the measurable cutoff frequency can be significantly extended. Therefore, our scheme has advantages in measuring broadband THz field over the common solid-based techniques. Our scheme can be realized efficiently with a probe laser energy 1 order of magnitude lower than the gas-based scheme. In other words, the sensitivity of our scheme is

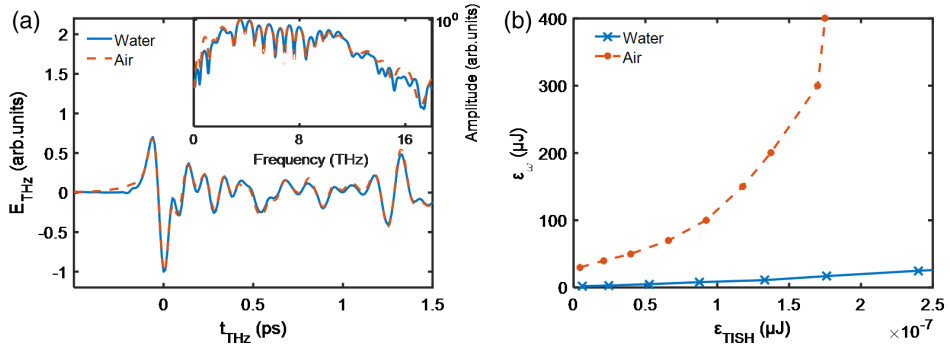

FIG. 4. Comparison of the water- and air-based detections. (a) THz time-domain waveforms and the corresponding spectra (inset). (b) Required probe beam energy to generate the TISH energy for the given THz field of 1 MV/cm. In each plot, the blue solid and red broken lines correspond to the results with the water- and air-based schemes, respectively.

1 order of magnitude. The sensitivity could be further enhanced by replacing other kinds of liquids with larger nonlinear susceptibility and lower absorption.

This work was supported by the Beijing Natural Science Foundation (Grant No. JQ18015), the National Key R&D Program of China (Grant No. 2018YFA0404801), National Natural Science Foundation of China (Grants No. 11775302, No. 12074272, No. 61935001, No. 61905271), the Strategic Priority Research Program of Chinese Academy of Sciences (Grants No. XDA25050300), the Fundamental Research Funds for the Central Universities, the Research Funds of Renmin University of China (20XNLG01), and the Guangdong Basic and Applied Basic Research Foundation (Grant No. 2020A1515011083).

*Corresponding author.
weiminwang1@ruc.edu.cn
†Corresponding author.
yjzhao@bit.edu.cn
‡Corresponding author.
liangliang_zhang@cnu.edu.cn
§These authors contributed equally to this work.

[1] H. Hoshina, A. Hayashi, N. Miyoshi, F. Miyamaru, and C. Otani, Terahertz pulsed imaging of frozen biological tissues, Appl. Phys. Lett. **94**, 123901 (2009).
[2] K. Wu, C. Qi, Z. Zhu, C. Wang, B. Song, and C. Chang, Terahertz wave accelerates DNA unwinding: A molecular dynamics simulation study, J. Phys. Chem. **11**, 7002 (2020).
[3] B. Born, H. Weingärtner, E. Bründermann, and M. Havenith, Solvation dynamics of model peptides probed by terahertz spectroscopy. Observation of the onset of collective network motions, J. Am. Chem. Soc. **131**, 3752 (2009).
[4] B. Ferguson and X. C. Zhang, Materials for terahertz science and technology, Nat. Mater. **1**, 26 (2002).
[5] Z. F. Chen, X. Q. Chen, L. Tao, K. Chen, M. Z. Long, X. D. Liu, K. Y. Yan, R. I. Stantchev, E. P. Macpherson, and J. B. Xu, Graphene controlled Brewster angle device for ultra broadband terahertz modulation, Nat. Commun. **9**, 1 (2018).
[6] M. Naftaly and R. E. Miles, Terahertz time-domain spectroscopy for material characterization, Proc. IEEE. **95**, 1658 (2007).
[7] L. L. Zhang, Z. F. Chen, R. Zhang, Y. Tan, T. Wu, M. Shalaby, R. Xie, and J. B. Xue, Direct observation of charge injection of graphene in the graphene/WSe_2 heterostructure by optical-pump terahertz-probe spectroscopy, ACS Appl. Mater. Interfaces **11**, 47501 (2019).
[8] R. A. Kaindl, M. A. Carnahan, D. Hagele, R. Lovenich, and D. S. Chemla, Ultrafast terahertz probes of transient conducting and insulating phases in an electron-hole gas, Nature (London) **423**, 734 (2003).
[9] M. Sajadi, M. Wolf, and T. Kampfrath, Transient birefringence of liquids induced by terahertz electric-field torque on permanent molecular dipoles, Nat. Commun. **8**, 14963 (2017).
[10] P. Zalden *et al.*, Molecular polarizability anisotropy of liquid water revealed by terahertz-induced transient orientation, Nat. Commun. **9**, 2142 (2018).
[11] E. Freysz and J. Degert, Nonlinear optics: Terahertz Kerr effect, Nat. Photonics **4**, 131 (2010).
[12] P. R. Smith, D. H. Auston, and M. C. Nuss, Subpicosecond photoconductive dipole antennas, IEEE J. Quantum Electron. **24**, 255 (1988).
[13] M. V. Exter and D. R. Grischkowsky, Characterization of an optoelectronic terahertz beam system, IEEE Trans. Microwave Theory Tech. **38**, 1684 (1990).
[14] Q. Wu and X. C. Zhang, Free-space electro-optic sampling of terahertz beams, Appl. Phys. Lett. **67**, 3523 (1995).
[15] Q. Wu and X. C. Zhang, 7 terahertz broadband GaP electro-optic sensor, Appl. Phys. Lett. **70**, 1784 (1997).
[16] A. Nahata, A. S. Weling, and T. F. A. Heinz, Wideband coherent terahertz spectroscopy system using optical rectification and electro-optic sampling, Appl. Phys. Lett. **69**, 2321 (1996).
[17] A. Leitenstorfer, S. Hunsche, J. Shah, M. C. Nuss, and W. H. Knox, Detectors and sources for ultrabroadband electro-optic sampling: Experiment and theory, Appl. Phys. Lett. **74**, 1516 (1999).
[18] G. Gallot and D. Grischkowsky, Electro-optic detection of terahertz radiation, J. Opt. Soc. Am. B **16**, 1204 (1999).
[19] S. Casalbuoni, H. Schlarb, B. Schmidt, P. Schmuser, B. Steffen, and A. Winter, Numerical studies on the electro-optic detection of femtosecond electron bunches, Phys. Rev. ST Accel. Beams **11**, 072802 (2008).
[20] H. Zhao, Y. Tan, L. L. Zhang, R. Zhang, C. L. Zhang, Y. J. Zhao, and X. C. Zhang, Ultrafast hydrogen-bond dynamics of liquid water revealed by terahertz-induced transient birefringence, Light Sci. Appl. **9**, 136 (2020).
[21] J. Dai, X. Xu, and X. C. Zhang, Detection of Broadband Terahertz Waves with a Laser-Induced Plasma in Gases, Phys. Rev. Lett. **97**, 103903 (2006).
[22] M. Woerner and K. Reimann, Harnessing terahertz polarization, Nat. Photonics **3**, 495 (2009).
[23] J. Liu, J. Dai, S. L. Chin, and X. C. Zhang, Broadband terahertz wave remote sensing using coherent manipulation of fluorescence from asymmetrically ionized gases, Nat. Photonics **4**, 1 (2010).
[24] N. Karpowicz *et al.*, Coherent heterodyne time-domain spectrometry covering the entire "terahertz gap", Appl. Phys. Lett. **92**, 011131 (2008).
[25] L. Chia-Yeh, V. S. Denis, Y. Zhou, and S. B. Mansoor, Broadband field-resolved terahertz detection via laser induced air plasma with controlled optical bias, Opt. Express **23**, 11436 (2015).
[26] X. Lu, N. Karpowicz, Y. Chen, and X. C. Zhang, Systematic study of broadband terahertz gas sensor, Appl. Phys. Lett. **93**, 261106 (2008).
[27] X. Lu, N. Karpowicz, Y. Chen, and X. C. Zhang, Broadband terahertz detection with selected gases, J. Opt. Soc. Am. B **26**, A66 (2009).
[28] J. L. Liu, J. M. Dai, X. Lu, I. C. Ho, and X. C. Zhang, Broadband terahertz wave generation, detection and coherent control using terahertz gas photonics, Int. J. High Speed Electron. Syst. **20**, 1100635 (2012).
[29] M. Kress, T. Loffler, S. Eden, M. Thomson, and H. G. Roskos, Terahertz-pulse generation by photoionization of air with laser pulses composed of both fundamental and second-harmonic waves, Opt. Lett. **29**, 1120 (2004).
[30] R. W. Boyd, *Nonlinear Optics* (Elsevier, Amsterdam, 2003).

[31] S. Minardi, A. Gopal, M. Tatarakis, A. Couairon, G. Tamošauskas, R. Piskarskas, A. Dubietis, and P. D. Trapani, Time-resolved refractive index and absorption mapping of light-plasma filaments in water, Opt. Lett. **33**, 86 (2008).

[32] J. Noack and A. Vogel, Laser-induced plasma formation in water at nanosecond to femtosecond time scales: Calculation of thresholds, absorption coefficients, and energy density, IEEE J. Quantum. Electron. **35**, 1156 (1999).

[33] A. Couairon and A. Mysyrowicz, Femtosecond filamentation in transparent media, Phys. Rep. **441**, 47 (2007).

[34] S. Minardi, C. Milian, D. Majus, A. Gopal, G. Tamosauskas, A. Couairon, T. Pertsch, and A. Dubietis, Energy deposition dynamics of femtosecond pulses in water, Appl. Phys. Lett. **105**, 224104 (2014).

[35] I. Dey, K. Jana, V. Y. Fedorov, A. D. Koulouklidis, A. Mondal, M. Shaikh, D. Sarkar, A. D. Lad, S. Tzortzakis, A. Couairon, and G. R. Kumar, Highly efficient broadband terahertz generation from ultrashort laser filamentation in liquids, Nat. Commun. **8**, 1184 (2017).

[36] Q. Jin, Y. E, K. Williams, J. Dai, and X. C. Zhang, Observation of broadband terahertz wave generation from liquid water, Appl. Phys. Lett. **111**, 071103 (2017).

[37] L. L. Zhang, W. M. Wang, T. Wu, S. J. Feng, K. Kang, C. L Zhang, Y. Zhang, Y. T. Li, Z. M. Sheng, and X. C Zhang, Strong terahertz radiation from a liquid-water line, Phys. Rev. Applied **12**, 014005 (2019).

[38] T. Wang, P. Klarskov, and P. U. Jepsen, Ultrabroadband THz time-domain spectroscopy of a free-flowing water film, IEEE Trans. Terahertz Sci. Technol. **4**, 425 (2014).

[39] See Supplemental Material at http://link.aps.org/supplemental/10.1103/PhysRevLett.128.093902 for detailed parameters of the THz source, CSH and liquid water film, coherent detection of 14.5 MV/cm THz field with different CSH energies, coherent detection of different THz fields with the CSH energy of 0.01 μJ, comparison of TISH energy in water- and air-based detection methods, coherent detection of 14.5 MV/cm THz field with different probe laser energies, recorded signals versus time delay and relative phase, detection sensitivity comparison between the water-based and the air-based schemes under the same experimental conditions, THz polarization sensitivity in the detection scheme, and influence of diffusion and recombination processes of plasma, which includes Ref. [40].

[40] F. Docchio, Lifetimes of plasmas induced in liquids and ocular media by single Nd: YAG laser pulses of different duration, Europhys. Lett. **6**, 407 (1988).